Optical Properties and Two-Dimensional Electronic Structure in Wide-Gap Layered Oxychalcogenide: $La_2CdO_2Se_2$

Hidenori Hiramatsu,*,† Kazushige Ueda,†,‡ Toshio Kamiya,†,§ Hiromichi Ohta,†,|| Masahiro Hirano,† and Hideo Hosono†,§

Hosono Transparent Electro-Active Materials (TEAM) Project, Exploratory Research for Advanced Technology (ERATO), Japan Science and Technology (JST) Agency, KSP C-1232, 3-2-1 Sakado, Takatsu, Kawasaki 213-0012, Japan, Materials and Structures Laboratory, Tokyo Institute of Technology, 4259 Nagatsuta, Midori, Yokohama 226-8503, Japan

Received: March 23, 2004; In Final Form: July 30, 2004

The optical and electronic properties of a wide-gap (~3.3 eV) layered oxychalcogenide, $La_2CdO_2Se_2$, were examined using epitaxial thin films prepared by a reactive solid-phase epitaxy. Two optical absorption peaks due to exciton split by the spin−orbit interaction were observed at 3.43 and 3.61 eV at 10 K near the absorption edge. A sharp ultraviolet photoluminescence was observed even at room temperature, indicating that the free exciton had a large binding energy (estimated value = ~40 meV) similar to Cu-based, layered oxychalcogenides LnCuOCh (Ln = lanthanide, Ch = chalcogen). The optical properties were compared to those of the Cu-based oxychalcogenides and low-dimensional CdSe-based materials. It is concluded that the two-dimensional crystal structure, which remarkably reduces the bandwidth of the conduction band, is a major origin for the wide band gap. Energy band calculations indicate that the holes are confined in the two-dimensional $(CdSe_2)^{2-}$ layer, which is most likely responsible for the large binding energy of the exciton.

1. Introduction

Artificial superlattice structures are widely used in practical optoelectronic devices such as a quantum well laser because carrier confinement on the nanometer scale remarkably improves device performances.[1] Generally, artificial superlattice structures are fabricated by time-consuming processes such as layer-by-layer growth techniques using molecular beam epitaxy or metal organic chemical vapor deposition, whereas there is a potential alternative approach to attain quantum confinement effects that utilize nanostructures naturally formed in crystals: compounds with layered crystal structures are possible candidates. For example, layered perovskites such as $La_{2-x}Ba_xCuO_4$[2,3] and $Bi_2Sr_2CaCu_2O_8$,[4,5] which include Cu−O planes, exhibit superconductivity. Carrier confinement effects are expected in such naturally formed layered structures when a constituent barrier layer has a large band offset and enough tunneling resistance to confine the carriers.

A series of Cu-based oxychalcogenides, LnCuOCh (Ln = lanthanide such as La, Pr, and Nd, Ch = chalcogen, S or Se) is also a layered material.[6−11] It is a wide-gap p-type semiconductor[12−14] that exhibits exceptional properties compared to representative wide-gap p-type semiconductors, which have already been applied to ultraviolet (UV)−green light emitting diodes (LEDs) utilizing pn junctions, like GaN:Mg[15] and ZnSe:N.[16] For instance, an exciton, an electron−hole pair, is stable at room temperature in the oxychalcogenides[13,14,17] and causes sharp, efficient UV−blue photoluminescence (PL).[18] In addition, the carrier transport properties can be controlled to exhibit metallic degenerate states while maintaining a large mobility, e.g., ~4 $cm^2\ V^{-1}\ s^{-1}$ in Mg-doped LaCuOSe.[19,20] LnCuOCh has a layered crystal structure that is composed of alternating $(Ln_2O_2)^{2+}$ and $(Cu_2Ch_2)^{2-}$ layers stacked along the *c*-axis, as shown in Figure 1a.[6−11] Regarding the layered structure as a "natural multiple-quantum-well" that consists of oxide barrier and chalcogenide well layers with monoatomic thickness, we recently revealed that the unique excitonic characteristics come from excitons/carriers confined in the naturally formed, two-dimensional electronic structure.[21] Thus, this type of layered oxychalcogenides is intensively studied, especially for use in optoelectronic devices[22−35] and optical switching devices that operate in the UV−blue region due to the room-temperature exciton and a large $\chi^{(3)}$ value.[36] To realize the devices, it is very important to find counterpart materials with different band gaps and carrier polarity. The combination of the materials enables us to fabricate double-hetero and pn junction structures that will dramatically improve the device performance. For this purpose, compounds having crystal structures similar to LnCuOCh have potential because they are favorable for forming good heteroepitaxial junctions.

Recently, we have developed a process for synthesizing a single-phase powder of a CdSe-based, layered oxychalcogenide $La_2CdO_2Se_2$.[37] Figure 1b shows the crystal structure of $La_2CdO_2Se_2$.[37,38] The CdSe-based oxychalcogenide has a layered structure composed of alternating stacks of $(La_2O_2)^{2+}$ and $(CdSe_2)^{2-}$ along the *c*-axis, similar to LnCuOCh, as shown in Figure 1a. The crystal symmetry is tetragonal, belonging to the space group $P4_2/nmc$ (No. 137).[37] The structural difference from LnCuOCh is that the Cd ions periodically occupy half of the

* Corresponding author. Tel: +81-44-850-9764. Fax: +81-44-819-2205. E-mail: h-hirama@lucid.msl.titech.ac.jp.

† Japan Science and Technology (JST) Agency. Present: Solution Oriented Research for Science and Technology (SORST), JST.

‡ Present address: Department of Materials Science, Faculty of Engineering, Kyushu Institute of Technology, 1-1 Sensui-cho, Tobata, Kitakyushu 804-8550, Japan.

§ Tokyo Institute of Technology.

|| Also with the Department of Molecular Design and Engineering, Graduate School of Engineering, Nagoya University, Furo-cho, Chikusa, Nagoya 464-8603, Japan.

10.1021/jp048722q CCC: $27.50
Published on Web 09/28/2004

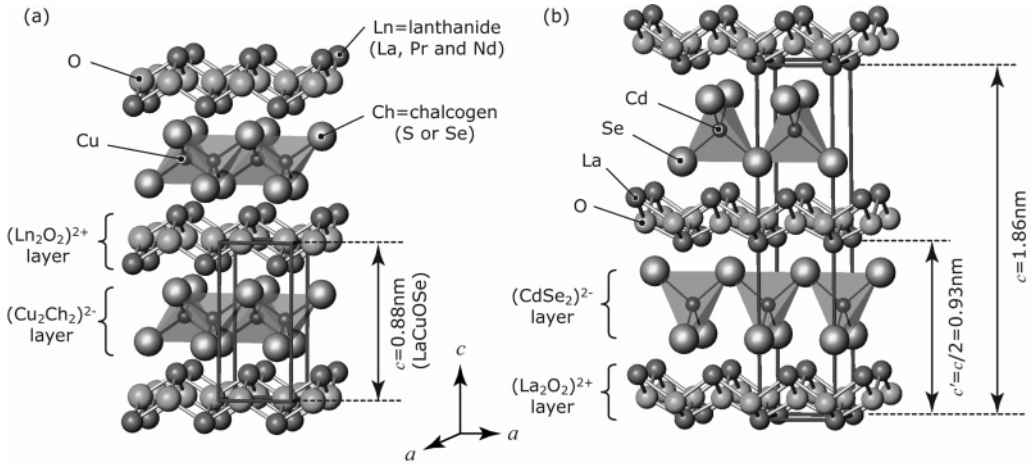

Figure 1. Crystal structures of layered oxychalcogenides: (a) LnCuOCh (Ln = lanthanide, La, Pr, and Nd; Ch = S or Se); (b) $La_2CdO_2Se_2$. Both crystals have tetragonal symmetry. Each layer of LnCuOCh consists of edge-shared Ln_4O and $CuCh_4$ tetrahedra, whereas that of $La_2CdO_2Se_2$ is composed of edge-shared La_4O and corner-shared $CdSe_4$ tetrahedra. Shadowed tetrahedra and rectangular solids show the tetrahedra of the chalcogenide layer and unit cells, respectively. The unit cell of $La_2CdO_2Se_2$ alternates stacks of two units of a fundamental cell (the length: $c' = c/2 = 0.93$ nm) rotated 90°, which forms a 2-fold superlattice structure in the *c*-axis direction via the 4_2 symmetry.

Cu sites in LnCuOCh. Thus, the $(CdSe_2)^{2-}$ layer in $La_2CdO_2Se_2$ is formed by corner-sharing $CdSe_4$ tetrahedra whereas the $(Cu_2Ch_2)^{2-}$ layer in LnCuOCh is formed by edge-sharing $CuCh_4$ tetrahedra. The unit cell of $La_2CdO_2Se_2$ is composed of two units of a fundamental cell with the length of $c' = c/2 = 0.93$ nm. Each fundamental cell is alternately stacked along the *c*-axis and is rotated by 90°, which forms a 2-fold superlattice structure in the [001] direction via the 4_2 symmetry. A difference in the point groups of the Se ions between LnCuOCh and $La_2CdO_2Se_2$ should be noticed for discussion on electronic structure: the Se ions in LnCuOCh occupy 4-fold symmetry sites, whereas the rotational symmetry of the Se ions in $La_2CdO_2Se_2$ is 2-fold symmetry. Each fundamental cell includes a $(CdSe_2)^{2-}$ layer. Therefore, the $(CdSe_2)^{2-}$ layers are stacked along the *c*-axis via the 4_2 symmetry and are rotated by 90°.

Measurements for a powder sample indicated that $La_2CdO_2Se_2$ did not exhibit electrical conduction and it had a band-gap energy as large as ~3.3 eV.[37] This band gap was unexpectedly large because CdSe has a small band gap (~1.8 eV) and the color of the previously reported sample was brownish.[38] The wide-gap feature of this CdSe-based oxychalcogenide may originate from the layered structure naturally formed in this crystal structure, as observed on the Cu-based layered oxychalcogenides.

In this Article, optical properties of high-quality heteroepitaxial thin films of $La_2CdO_2Se_2$ are examined. The band gap is confirmed to be ~3.3 eV at room temperature. Furthermore, it exhibits excitonic optical absorption and PL even at room temperature. The wide-gap feature and the large binding energy of the exciton of this CdSe-based oxychalcogenide are discussed in relation to the crystal structure and the naturally formed two-dimensional structure with an aid of ab initio band calculations. Further, they are compared with those of nanometer-sized CdSe-based materials.

2. Experimental Section

2.1. Preparation of Epitaxial Thin Film. $La_2CdO_2Se_2$ heteroepitaxial thin films (thickness ~150 nm) were prepared on MgO (001) single-crystal substrates (size: 10 mm × 10 mm square x 0.5 mm thickness) by a reactive solid-phase epitaxy (R-SPE) method.[39,40] In this process, pre-deposited thick amorphous films were crystallized by thermally annealing with the assistance of a very thin sacrificial layer, which controlled the crystallographic heteroepitaxial orientation through solid-state epitaxial growth (see Figure 2 for a schematic diagram). This method is advantageous because epitaxial growth conditions may be chosen independently from the film deposition conditions, which allows better process controllability for preparing high-quality epitaxial films especially for materials composed of high vapor pressure elements such as LnCuOCh.[41−43]

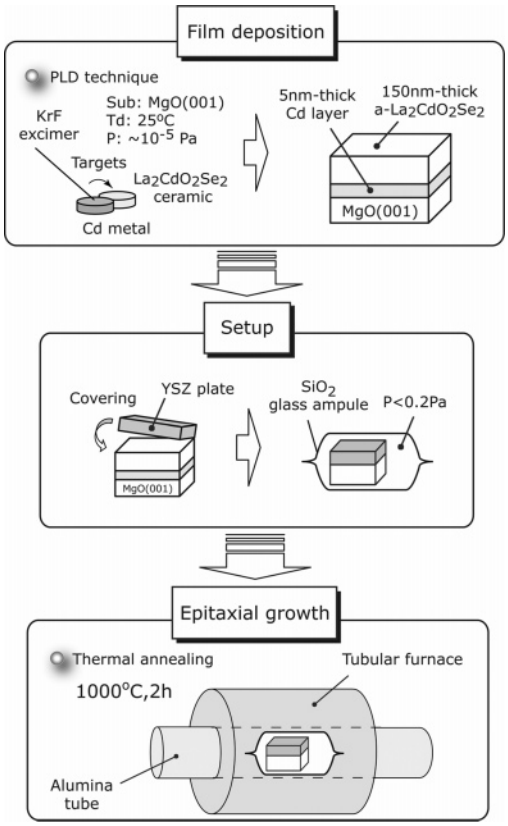

Figure 2. Process flow of R−SPE for synthesizing $La_2CdO_2Se_2$ epitaxial film.

A pulsed laser deposition (PLD) technique was employed for depositing the thin films because a PLD technique easily reproduces the chemical composition of target materials in the

deposited films when a low growth temperature is used. The PLD chamber was specifically designed for the epitaxial growth of chalcogenides.[44] A KrF excimer laser (wavelength 248 nm, apparatus COMPex102 made by LAMBDA PHYSIK, power density ~2 J cm^{-2} $pulse^{-1}$, repetition 10 Hz) was used to ablate PLD targets. A bilayer film structure of amorphous (a-) $La_2CdO_2Se_2$ (thickness ~150 nm)/Cd (~5 nm) on MgO (001) substrate was initially prepared by PLD using Cd metal and $La_2CdO_2Se_2$ ceramic disks (20 mm in diameter and 5 mm thick) as the PLD targets. Each layer was sequentially deposited under a vacuum (~10^{-5} Pa) at ~25 °C. Then, the bilayer film was covered with an yttria-stabilized zirconia (YSZ) plate and sealed in an evacuated SiO_2 glass ampule at <0.2 Pa with a small amount of $La_2CdO_2Se_2$ powder to control the firing atmosphere, which was subsequently annealed at 1000 °C for 2 h. Finally, the sample was removed from the SiO_2 glass ampule at room temperature in air. It was confirmed that the film did not react with the YSZ cover plate and a clean film surface was maintained.

2.2. Characterization. The crystallographic orientation and crystallinity of the $La_2CdO_2Se_2$ epitaxial films were examined by four-axes high-resolution X-ray diffraction measurements (HRXRD, apparatus model ATX-G, RIGAKU-Co., radiation monochromatic Cu Kα_1, wavelength 1.54056 Å, power 50 kV and 300 mA) at room temperature. Out-of-plane ($\omega-2\theta$ synchronous scan) and in-plane ($\phi-2\theta\chi$ synchronous scan) measurements determined the crystallographic orientations parallel and perpendicular to the substrate surface, respectively. Out-of-plane rocking curve (2θ-fixed ω scan) and in-plane rocking curve ($2\theta\chi$-fixed ϕ scan) measurements estimated the tilting and twisting angles of crystallite orientations. The surface morphology was observed using an atomic force microscope (AFM, apparatus SPI-3800N made by SII) at room temperature.

PL spectra were measured between 10 and 300 K using a spectrometer with a charge-coupled device detector and the excitation was from a He−Cd laser (wavelength 325 nm, power density ~30 mW cm^{-2}). A conventional spectrophotometer (model U-4000, HITACHI-Co.) measured the optical absorption spectra in the same temperature range.

The electronic structure was calculated with an ab initio linearized augmented plane wave/augmented plane wave + local orbitals (LAPW/APW+lo) method, WIEN2k code using the PBE96 GGA function with the spin−orbit interaction at a semirelativistic level.[45] Similar calculations were also performed using CASTEP (ACCELRYS K.K.) at a nonrelativistic level without the spin−orbit interaction to confirm the results from WIEN2k. The band and density of states (DOS) structures obtained by both codes were consistent with each other except for band splitting due to the spin−orbit interaction. Consequently, the WIEN2k results are used for the discussion.

3. Results and Discussion

3.1. Heteroepitaxially Grown Thin Film. It should be noted that using the thin, sacrificial Cd layer is a key for heteroepitaxial growth during thermal annealing in R-SPE. [42] When the Cd layer was not deposited between the a-$La_2CdO_2Se_2$ layer and MgO substrate, the obtained films were polycrystalline with a large orientation fluctuation of small crystallites. It is favorable to deposit the a-$La_2CdO_2Se_2$ layer at a low temperature such as ~25 °C because the constituent elements, especially Cd and Se, have high vapor pressures and re-evaporate from the deposited films if a sample is subjected to a higher temperature in a vacuum.

When the thin sacrificial Cd layer is used, the a-$La_2CdO_2Se_2$ film is converted to an epitaxial film by thermal annealing,

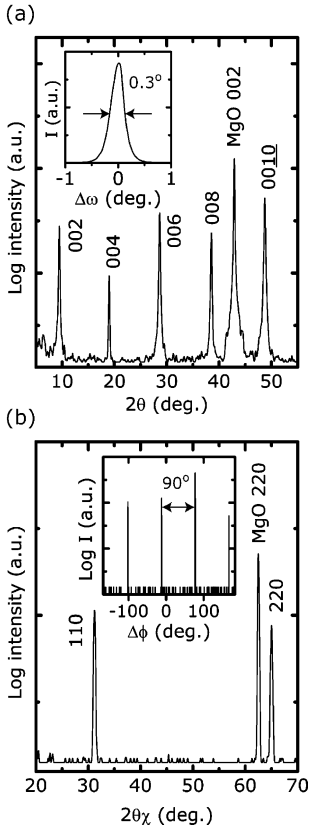

Figure 3. (a) Out-of-plane and (b) in-plane HRXRD patterns of the $La_2CdO_2Se_2$ epitaxial film prepared on MgO (001) substrate. Insets show (a) 2θ-fixed ω scan at the 006 diffraction and (b) $2\theta\chi$-fixed ϕ scan at the 220 diffraction.

similar to LnCuOCh.[41−43] Figure 3a shows the out-of-plane HRXRD pattern of the $La_2CdO_2Se_2$ film prepared by R-SPE. Only sharp 00*l* diffraction peaks from $La_2CdO_2Se_2$ are observed with the MgO 002 diffraction, indicating that the film is strongly *c*-axis oriented normal to the substrate surface. The full width at half-maximum (FWHM) of the 006 diffraction peak is as small as 0.09°. The inset shows that the FWHM of the out-of-plane rocking curve (2θ-fixed ω scan) is rather large (0.3°), which may be due to the large difference in thermal expansion coefficients between $La_2CdO_2Se_2$ and MgO. The in-plane HRXRD measurements examined the in-plane orientation of the crystallites (Figure 3b). It exhibited only sharp *hk*0 diffractions of $La_2CdO_2Se_2$ and MgO, and 4-fold $La_2CdO_2Se_2$ 220 diffraction peaks that appear in the $2\theta\chi$-fixed ϕ scan, as shown in the inset of Figure 3b. The FWHM value of the ϕ scan peaks was 0.4°. These results indicate that the $La_2CdO_2Se_2$ film heteroepitaxially grows on the MgO substrate with the crystallographic orientation of (001)[110] $La_2CdO_2Se_2$ || (001)[110] MgO. An AFM image of the film surface (Figure 4) suggests that the crystallites in the film are relaxed. Strongly oriented, tetragonal facets are clearly observed with the orientation, which is consistent with the crystallographic orientation determined by HRXRD. The root-mean-square roughness and lateral grain size were ~5 and ~500 nm, respectively.

3.2. Optical Properties. Figure 5a shows the optical absorption and PL spectra measured at 10 K. Two absorption peaks were observed at 3.43 and 3.61 eV near the absorption edge. The peak split (denoted S.O.) results from the spin−orbit interaction of Se ion at the valence band maximum (VBM) state similar to Cu-based oxychalcogenides,[21] which will be discussed in the next section. Three sharp emission peaks at 3.42 eV (denoted FE), 3.28 eV (BE_1), and 3.30 eV (BE_2) were observed

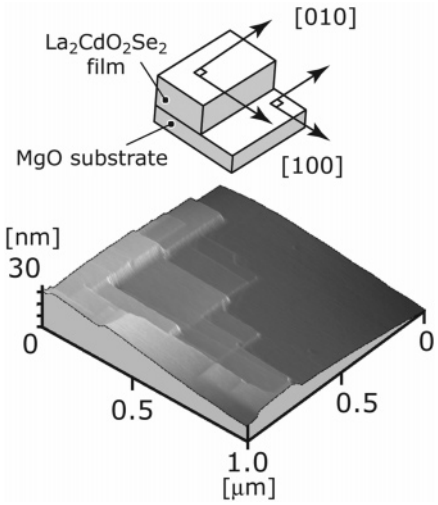

Figure 4. AFM image of the $La_2CdO_2Se_2$ epitaxial film. The top figure illustrates the relationship between the orientation of MgO and that of the crystallite facet in the film.

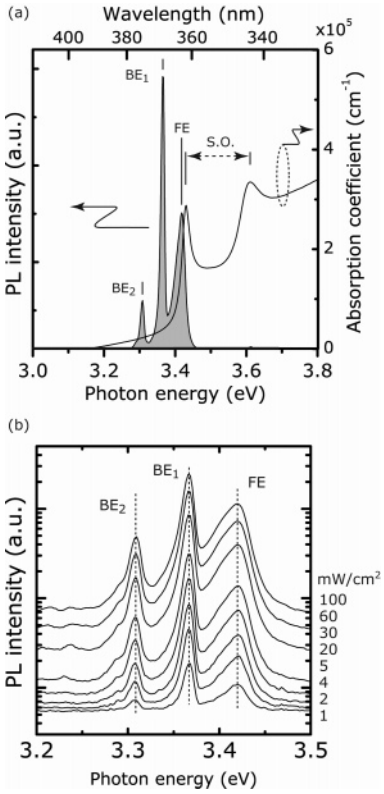

Figure 5. (a) Optical absorption and PL spectra at 10 K. S.O. indicates a split of the absorption band due to the spin−orbit interaction. (b) Excitation power dependence of PL spectra at 10 K on a logarithm scale. Excitation powers are shown at right of the figure.

in the PL spectrum. The emission energy of 3.42 eV is very close to the lower energy of the absorption peaks (3.43 eV), indicating that the FE emission comes from a free exciton. The energies of all the PL peaks do not shift with the excitation power, as shown in Figure 5b, suggesting that the other emission peaks (BE_1 and BE_2) are not due to donor−acceptor pairs but may be assigned to bound excitons. The blue shift in the PL peaks and the absorption edges as the temperature decreases, as shown in Figures 6 and 7, respectively, support this assignment.

Figure 6 shows the variations of the PL spectra with temperature. Figure 7 summarizes the peak energies of the PL

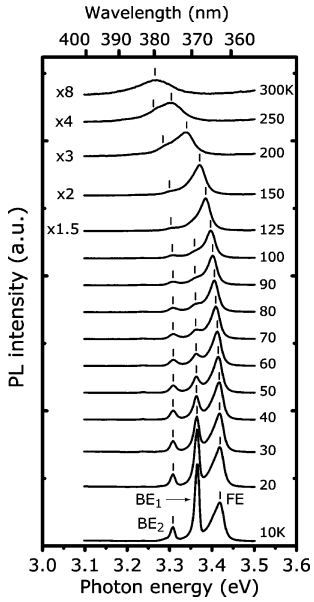

Figure 6. Temperature dependence of PL spectra near the absorption edge. Magnifications and measurement temperatures are shown at left and right of each spectrum.

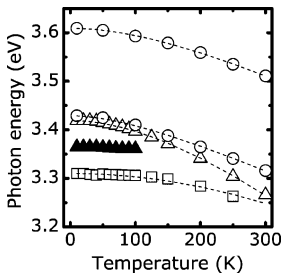

Figure 7. Temperature dependence of peak energies of absorption (open circles), FE emission (open triangles), BE_1 emission (closed triangles), and BE_2 emission (open squares). The dotted curves show the results fitted using Varshni's empirical model.

and the corresponding absorption as a function of temperature. The dotted curves are the results fitted using Varshni's empirical relationship.[46] Blue shifts are observed for the FE, BE_1, and BE_2 emissions and the free exciton absorption. The BE_1 and BE_2 peak energies are respectively smaller by ∼50 and ∼110 meV than the FE energy. This large energy difference is consistent with that in the temperature where the excitonic emission is washed out (100 K for BE_1 and 250 K for BE_2); i.e., the bound excitons are tightly bound. The FE emission (3.27 eV) and absorption (3.32 eV) peaks are clearly observed even at 300 K, indicating that the binding energy of the free exciton is larger than the room-temperature thermal energy (26 meV). The binding energy was estimated from the temperature dependence of the PL intensities using a thermal decomposition model,[47,48] which gave a binding energy as large as ∼40 meV, comparable to that of LaCuOCh (∼50 meV).[19]

As the exciton absorption strongly overlaps on the fundamental band gap, the absorption edge energy (∼3.3 eV) was used to measure the band gap at room temperature. The absorption edge energy is consistent with that obtained by diffuse reflectance measurement on the powder sample at room temperature.[37] It is noteworthy that $La_2CdO_2Se_2$ has larger band-gap energy than those of Cu-based, layered oxychalcogenides reported to date (e.g., 3.1 eV for LaCuOS and 2.8 eV for LaCuOSe[13]).

3.3. Electronic Structure. Here, the above results are discussed on the basis of the electronic structure that incorpo-

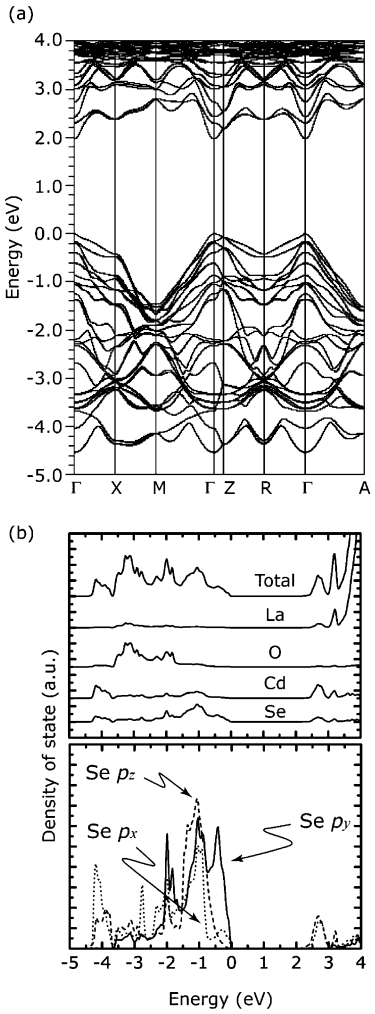

Figure 8. Electronic structure of $La_2CdO_2Se_2$ calculated by the LAPW/APW+lo method. (a) Band structure and (b) total and projected density of states (PDOS) for constituent atoms (top). Bottom of (b) shows PDOS of Se 4p states and *x*, *y*, and *z* show the local coordinates, respectively.

rates the spin−orbit interaction calculated by an ab initio LAPW/APW+lo method. Figure 8a shows the band structure of $La_2CdO_2Se_2$, which demonstrates that $La_2CdO_2Se_2$ is a direct transition-type semiconductor in which the VBM and conduction band minimum (CBM) states are located at the Γ point. The calculated band-gap energy is ∼1.97 eV, which is much smaller than the observed value (∼3.3 eV) because the density-functional theory underestimates the band gaps. Therefore, the calculated value is relatively compared to those for LaCuOS (1.65 eV) and LaCuOSe (1.49 eV) and the order of the band-gap energies agree with the previously observed results.[13]

Figure 8b shows total and projected density of states (PDOSs) for all the constituent atoms (upper) and for Se $4p_x$, p_y and p_z orbitals (lower). Note that X_G, Y_G, and Z_G (Figure 9a) denote the global coordinates of the lattice, and *x*, *y*, and *z* represent the local coordinates that belong to a Se ion. The Se ion has 2-fold symmetry, and Se and Cd ions form a one-dimensional Se−Cd−Se zigzag chain along the X_G or Y_G axes according to the fundamental unit cells [see the red lines and the local coordinates shown on Se ions in Figure 9b]. The local coordinate *x* is by definition parallel to the direction of the zigzag chain. Therefore, the local coordinates on a Se ion are rotated 90° by translating along the *c*-axis. It is determined that the VBM state is mainly from the Se p_y states, and that Se p_x, p_z states are located deeper by >0.8 eV. The CBM state is mainly composed of Cd 5s orbitals. These features are different from those in LaCuOSe, where the VBM state is composed of Se p_y states largely hybridized with Cu 3d,[21] forming a hole conduction path in the $(Cu_2Se_2)^{2-}$ layer spread to Se and Cu ions. In contrast, due to the 2-fold point-group symmetry at the Se site,[37,38] the Se $4p_x$ and p_y levels are split, where the former forms Cd−Se bonds by slightly mixing of Cd 5*p* to Se $4p_x$, p_y, p_z orbitals, and the latter forms the VBM state composed almost only of Se $4p_y$.

Figure 9a demonstrates this picture more clearly, where electron density at the VBM state is plotted superimposed on the crystal structure of $La_2CdO_2Se_2$ (the figure was prepared using XCrySDen[49]). The VBM Se $4p_y$ states extend to neighboring Se ions in the *y*-direction and forms Se $4p_y$ σ^* antibonding state (see "B" in Figure 9), but much less electron density is found between Cd and Se ions in the Se−Cd−Se zigzag chain. This result is reasonable because the Se $4p_y$ σ^* is an antibonding state extending normal to the Se−Cd−Se zigzag chain. These bonding natures are also seen in the band structure (Figure 8a). The bands near the VBM sate are classified into two groups; i.e., one has small band dispersion (heavy hole band), and the other has much larger dispersion (light hole band) along the Γ−X direction. Note that the Se $4p_y$ states form two different bonds at *k* points (coordinate in the reciprocal space is denoted k_x hereafter) in the Γ−X direction due to the 4_2 symmetry. One is a π^*-like bond and the other is a σ^*-like bond. These are degenerate at the Γ point, but split at finite k_x. The heavy hole band along the Γ−X direction is attributed to the π^*-like bond and the light hole band is the σ^*-like bond.

If the spin−orbit interaction is not considered, then the VBM states at the Γ point are only split into two levels with an energy spacing of ∼0.2 eV and the energy split results from the double period superlattice structure of $La_2CdO_2Se_2$. The spin−orbit interaction further splits these levels by ∼0.18 eV. Consequently, the VBM states at the Γ point are split with an energy spacing of ∼0.2 eV each, which results in the three split VBM states between −0.6 and 0.0 eV in the band structure (Figure 8). The calculated spin−orbit energy split of ∼0.2 eV is consistent with the energy split between the two absorption peaks in Figure 5a (denoted S. O.). The observed energy split is ∼180 meV, which is larger than those of other oxychalcogenides such as LaCuOSe (∼125 meV) [21] and suggests that the contribution of Cd orbitals to the VBM state via hybridization is much smaller than that of Cu in LaCuOSe. This prospect is consistent with that the VBM state is composed almost only of Se $4p_y$ state.

3.4. Origin of the Large Band Gap and the Large Exciton Binding Energy. In comparison of $La_2CdO_2Se_2$ with CdSe, the neighboring Cd−Cd and Se−Se distances (both are 0.41 nm) in $La_2CdO_2Se_2$ are almost the same as those in CdSe (0.43 nm). Therefore, the overlap of the wave function between neighboring Cd−Cd or Se−Se does not differ significantly in these compounds. On the other hand, the coordination number of Se ion in $La_2CdO_2Se_2$ becomes smaller than that in CdSe; two in $La_2CdO_2Se_2$ and four in CdSe because $CdSe_4$ tetrahedra in $La_2CdO_2Se_2$ are connected only in a one-molecular-layer. This difference in the local structure around the Se ion might make a difference in the electronic structure of valence band (VB) between $La_2CdO_2Se_2$ and CdSe and may influence the bandwidth of VB. However, the band calculation shows that the VB has a wide bandwidth (∼4.5 eV), whereas the conduction band (CB) has a small dispersion, only ∼2 eV in width (Figure 8a). The band structure of wurtzite-type (6H) CdSe was also calculated for comparison. It gave the conduction bandwidth of ∼4 eV, which is much larger than that of $La_2CdO_2Se_2$. The

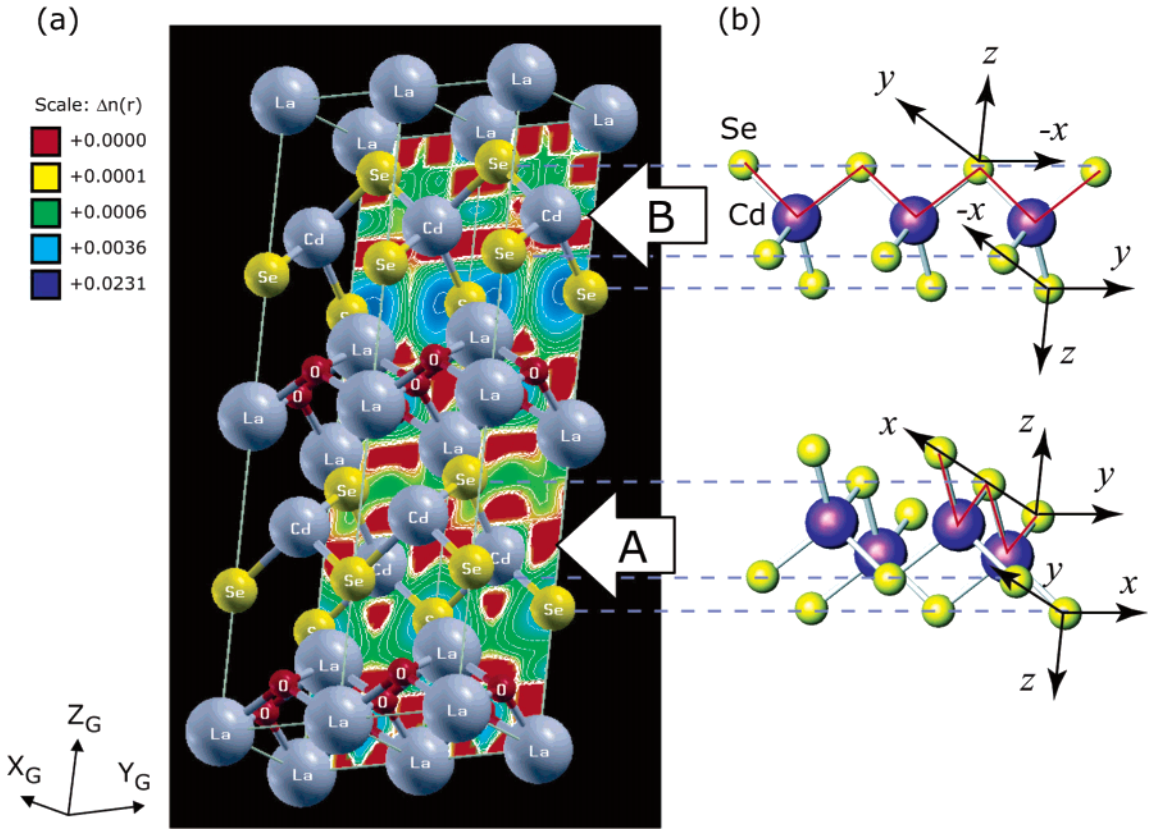

Figure 9. (a) Electron density map at the VBM state plotted on the Y_G-Z_G plane intersecting the (100) plane of $La_2CdO_2Se_2$. X_G, Y_G, and Z_G show the global coordinates, respectively. $CdSe_2$ layer "A" includes Se ions forming the Se−Cd−Se zigzag chain perpendicular to the Y_G-Z_G plane, whereas $CdSe_2$ layer "B" includes Se ions forming the Se−Cd−Se zigzag chain along the Y_G-axis. (b) The $CdSe_2$ layers are extracted on the right for clarity. The corresponding zigzag chains are shown by red lines and the local coordinates associated with Se ions are shown by *x*, *y*, and *z*, which are turned 90° between "A" and "B" due to the 4_2 symmetry. The local coordinate, *x*, defines the direction of the zigzag chain.

bandwidth of VB is ∼4 eV, which is almost the same as that in $La_2CdO_2Se_2$. These results indicate that the large band gap of $La_2CdO_2Se_2$ is primarily attributed to the small dispersion of the Cd 5s CB. The small dispersion of CB gives rise to a difficulty in the impurity doping in $La_2CdO_2Se_2$.[37] Because the energy level of the CBM state is higher than those of other oxychalcogenides and CdSe-based materials, deeper donor levels may be formed by impurity doping and/or deep defects that trap the generated electrons, leading to poor ionization efficiency of the donor.

It is generally accepted[50] that overlap between cation's orbitals is important to determine the bandwidth of CB in wide gap n-type semiconductors; the bandwidth of CB increases as the overlap increases. The overlap is also critical for the formation of the n-type electrical conduction path. In $La_2CdO_2Se_2$, a semiconducting $(CdSe_2)^{2-}$ layer intervenes between insulating $(La_2O_2)^{2+}$ layers in the *c*-axis direction. This crystal structure reduces the interlayer hybridization of Cd 5s orbitals and thus the Cd 5s hybridization within a $(CdSe_2)^{2-}$ layer becomes dominant to form the CB. These considerations indicate that the large band gap of $La_2CdO_2Se_2$ primarily originates from the layered structure of this material.

Because the band gap of $La_2CdO_2Se_2$ is determined by the $(CdSe_2)^{2-}$ layers (i.e., the CBM state is mainly composed of Cd 5s and the VBM state of Se 4p), we compared the band-gap energies and exciton binding energies of $La_2CdO_2Se_2$ with those of CdSe-based materials, a bulk single crystal (three-dimensional crystal),[51,52] a CdSe/CdS artificial superlattice (two-dimensional crystal),[53] and a nanocrystal (zero-dimensional crystal).[54] Table 1 summarizes absorption edge energies at room temperature, a measure of the band gap energy, of the CdSe-based materials and Cu-based oxychalcogenides LaCuOCh,[13,18] in which band gaps are determined by $(Cu_2Ch_2)^{2-}$ layers. It is reported that the band gap of the CdSe-based material strongly depends on its dimensionality and size due to the quantum confinement effect.[54] For instance, the band-gap energy of the CdSe nanocrystal increases from 1.8 eV (three-dimensional bulk) to 2.9 eV (zero-dimensional nanocrystal), approaching the band-gap energy of $La_2CdO_2Se_2$ (∼3.3 eV), as shown in Figure 10. The band-gap energy of $La_2CdO_2Se_2$ is as large as that of nanocrystalline CdSe with a particle size of ∼1 nm, which suggests that the quantum confinement effect may be also considered to fully understand the large band gap of $La_2CdO_2Se_2$.

TABLE 1: Summary of Absorption Edge Energies at 300 K and the Exciton Binding Energy for $La_2CdO_2Se_2$, the Cu-Based Oxychalcogenides LnCuOCh (Ln = Lanthanide, Ch = Chalcogen), and Various CdSe Samples (3D, Bulk Single Crystal; 2D, CdSe/CdS Superlattice; 0D, Nanoparticles, Particle Size ∼1.2 nm)

material	absorption edge energy (eV)	exciton binding energy (meV)
$La_2CdO_2Se_2$	3.3	40
LaCuOS	3.1	50
LaCuOSe	2.8	50
CdSe (bulk single crystal, 3D)	1.8	15
CdSe (CdSe/CdS superlattice, 2D)	–	42
CdSe (nanoparticles, 0D)	2.9	–

The two-dimensional structure may be also related to the large binding energy of the exciton. Table 1 demonstrates that the exciton binding energy of the CdSe-based material increases as the dimensionality decreases. It also shows that a large value of 42 meV, which is comparable to that of $La_2CdO_2Se_2$, is

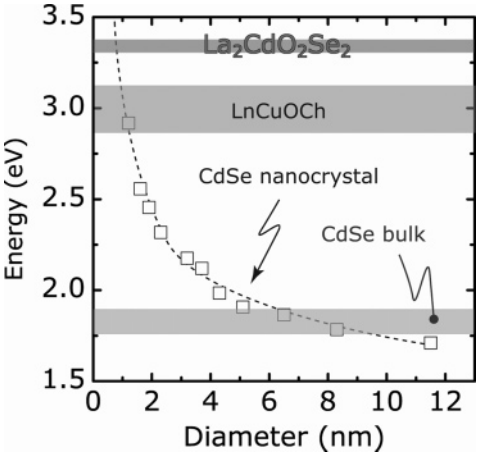

Figure 10. Comparison of absorption edge energy (~3.3 eV) of $La_2CdO_2Se_2$ at room temperature with those of other CdSe-based materials (0D, CdSe nanocrystals with various particle sizes; 3D, bulk single crystal). Zonal data (2.8−3.1 eV) of layered oxychalcogenides LnCuOCh (Ln = lanthanides such as La, Pr, and Nd, Ch = chalcogens, S or Se) are shown for comparison.

obtained for the CdSe/CdS superlattice (two-dimensional exciton). The electron density at the VBM state in Figure 9a indicates holes are confined in the $(CdSe_2)^{2-}$ layer in $La_2CdO_2Se_2$. Therefore, we consider that the large binding energy of exciton in $La_2CdO_2Se_2$ comes from the carrier and/or exciton confinement effect that originates from the two-dimensional electronic structure composed of monoatomic oxide $(La_2O_2)^{2+}$ barrier and chalcogenide $(CdSe_2)^{2-}$ well layers, which is similar to LnCuOCh.[21]

4. Conclusion

Epitaxial thin films of $La_2CdO_2Se_2$ on MgO (001) single-crystal substrates were fabricated by a reactive solid-phase epitaxy. Structural analyses revealed that the obtained films were heteroepitaxially grown on MgO substrates. The films of $La_2CdO_2Se_2$ had a large band-gap energy of ~3.3 eV, which was larger than Cu-based, layered oxychalcogenides LnCuOCh (Ln = lanthanide, Ch = chalcogen) reported to date. One free and two bound excitonic emissions were clearly observed, together with the free excitonic absorption, confirming that the fabricated films have good quality. The excitons in $La_2CdO_2Se_2$ were stable even at room temperature, similar to the Cu-based oxychalcogenides. The estimated exciton binding energy was ~40 meV. These optical properties were discussed in relation to the layered crystal structure. The two-dimensional crystal structure remarkably reduces the bandwidth of the conduction band, leading to the wide band-gap energy of this material. Furthermore, it is revealed that holes are confined in the two-dimensional $(CdSe_2)^{2-}$ layer. The large binding energy of the exciton may be due to the confinement effects. Although $La_2CdO_2Se_2$ does not exhibit good electrical conduction, its insulating nature and the band gap larger than LnCuOCh are favorable for building blocks of optoelectronic devices such as an electron blocking layer in double-hetero junction LEDs and a light-emitting layer in p/i/n LEDs.

References and Notes

(1) Zory, P. S., Jr. *Quantum Well Laser*; Academic Press: New York, 1993.

(2) Bednorz, J. G.; Müller, K. A. *Z. Phys. B* **1986**, *64*, 189.

(3) Müller, K. A.; Takashige, M.; Bednorz, J. G. *Phys. Rev. Lett.* **1987**, *58*, 1143.

(4) Sunshine, S. A.; Siegrist, T.; Schneemeyer, L. F.; Murphy, D. W.; Cava, R. J.; Batlogg, B.; van Dover: R. B.; Fleming, R. M.; Glarum, S. H.; Nakahara, S.; Farrow, R.; Krajewski, J. J.; Zahurak, S. M.; Waszczak, J. V.; Marshall, J. H.; Marsh, P.; Rupp, L. W., Jr.; Peck, W. F. *Phys. Rev. B* **1988**, *38*, 893.

(5) Subramanian, M. A.; Torardi, C. C.; Calabrese, J. C.; Gopalakrishnan, J.; Morrissey, K. J.; Askew, T. R.; Flippen, R. B.; Chowdhry, U.; Sleight, A. W. *Science* **1988**, *239*, 1015.

(6) Palazzi, M.; Carcaly, C.; Flahaut, J. *J. Solid State Chem.* **1980**, *35*, 150.

(7) Palazzi, M. *C. R. Acad. Sci. Paris* **1981**, *292*, 789.

(8) Zhu, W. J.; Huang, Y. Z.; Dong, C.; Zhao, Z. X. *Mater. Res. Bull.* **1994**, *29*, 143.

(9) Kusainova, A. M.; Berdonosov, P. S.; Aksel'rud, L. G.; Kholodkovskaya, L. N.; Dolgikh, V. A.; Popovkin, B. A. *J. Solid State Chem.* **1994**, *112*, 189.

(10) Popovkin, B. A.; Kusainova, A. M.; Dolgikh, V. A.; Aksel'rud, L. G. *Russ. J. Inorg. Chem.* **1998**, *43*, 1471.

(11) Charkin, D. O.; Akopyan, A. V.; Dolgikh, V. A. *Russ. J. Inorg. Chem.* **1999**, *44*, 833.

(12) Ueda, K.; Inoue, S.; Hirose, S.; Kawazoe, H.; Hosono, H. *Appl. Phys. Lett.* **2000**, *77*, 2701.

(13) Ueda, K.; Hosono, H. *J. Appl. Phys.* **2002**, *91*, 4768.

(14) Ueda, K.; Takafuji, K.; Hiramatsu, H.; Ohta, H.; Kamiya, T.; Hirano, M.; Hosono, H. *Chem. Mater.* **2003**, *15*, 3692.

(15) Akasaki, I.; Amano, H. *Jpn. J. Appl. Phys.* **1997**, *36*, 5393.

(16) Itoh, S.; Ishibashi, A. *SPIE Proc.* **1994**, *2346*, 2.

(17) Ueda, K.; Inoue, S.; Hosono, H.; Sarukura, N.; Hirano, M. *Appl. Phys. Lett.* **2001**, *78*, 2333.

(18) Hiramatsu, H.; Ueda, K.; Takafuji, K.; Ohta, H.; Hirano, M.; Kamiya, T.; Hosono, H. *J. Appl. Phys.* **2003**, *94*, 5805.

(19) Hiramatsu, H.; Ueda, K.; Ohta, H.; Hirano, M.; Kamiya, T.; Hosono, H. *Appl. Phys. Lett.* **2003**, *82*, 1048.

(20) Hiramatsu, H.; Ueda, K.; Ohta, H.; Hirano, M.; Kamiya, T.; Hosono, H. *Thin Solid Films* **2003**, *445*, 304.

(21) Ueda, K.; Hiramatsu, H.; Ohta, H.; Hirano, M.; Kamiya, T.; Hosono, H. *Phys. Rev. B* **2004**, *69*, 155305.

(22) Ishikawa, K.; Kinoshita, S.; Suzuki, Y.; Matsuura, S.; Nakanishi, T.; Aizawa, M.; Suzuki, Y. *J. Electrochem. Soc.* **1991**, *138*, 1166.

(23) Takano, Y.; Yahagi, K.; Sekizawa, K. *Physica B* **1995**, *206 & 207*, 764.

(24) Ueda, K.; Hirose, S.; Kawazoe, H.; Hosono, H. *Chem. Mater.* **2001**, *13*, 1880.

(25) Hiramatsu, H.; Orita, M.; Hirano, M.; Ueda, K.; Hosono, H. *J. Appl. Phys.* **2002**, *91*, 9177.

(26) Hiramatsu, H.; Ueda, K.; Ohta, H.; Orita, M.; Hirano, M.; Hosono, H. *Thin Solid Films* **2002**, *411*, 125.

(27) Hirose, S.; Ueda, K.; Kawazoe, H.; Hosono, H. *Chem. Mater.* **2002**, *14*, 1037.

(28) Takase, K.; Koyano, M.; Shimizu, T.; Makihara, K.; Takahashi, Y.; Takano, Y.; Sekizawa, K. *Solid State Commun.* **2002**, *123*, 531.

(29) Sato, H.; Negishi, H.; Wada, A.; Ino, A.; Negishi, S.; Hirai, C.; Namatame, H.; Taniguchi, M.; Takase, K.; Takahashi, Y.; Shimizu, T.; Takano, Y.; Sekizawa, K. *Phys. Rev. B* **2003**, *68*, 035112.

(30) Ueda, K.; Takafuji, K.; Hosono, H. *J. Solid State Chem.* **2003**, *170*, 182.

(31) Yanagi, H.; Tate, J.; Park, S.; Park, C.-H.; Keszler, D. A. *Appl. Phys. Lett.* **2003**, *82*, 2814.

(32) Clarke, S. J.; Denis, S. G.; Rutt, O. J.; Hill, T. L.; Hayward, M. A.; Hyett, G.; Gál, Z. A. *Chem. Mater.* **2003**, *15*, 5065.

(33) Yanagi, H.; Park, S.; Draeseke, A. D.; Keszler, D. A.; Tate, J. *J. Solid State Chem.* **2003**, *175*, 34.

(34) Hyett, G.; Rutt, O. J.; Gál, Z. A.; Denis, S. G.; Hayward, M. A.; Clarke, S. J. *J. Am. Chem. Soc.* **2004**, *126*, 1980.

(35) Hiramatsu, H.; Ueda, K.; Takafuji, K.; Ohta, H.; Hirano, M.; Kamiya, T.; Hosono, H. *Appl. Phys. A* **2004**, *79*, 1521.

(36) Kamioka, H.; Hiramatsu, H.; Ohta, H.; Hirano, M.; Ueda, K.; Kamiya, T.; Hosono, H. *Appl. Phys. Lett.* **2004**, *84*, 879.

(37) Hiramatsu, H.; Ueda, K.; Kamiya, T.; Ohta, H.; Hirano, M.; Hosono, H. *J. Mater. Chem.* **2004**, *14*, 2946.

(38) Baranov, I. Yu.; Dolgikh, V. A.; Popovkin, B. A. *Russ. J. Inorg. Chem.* **1996**, *41*, 1819.

(39) Ohta, H.; Nomura, K.; Orita, M.; Hirano, M.; Ueda, K.; Suzuki, T.; Ikuhara, Y.; Hosono, H. *Adv. Funct. Mater.* **2003**, *13*, 139.

(40) Nomura, K.; Ohta, H.; Ueda, K.; Orita, M.; Hirano, M.; Hosono, H. *Thin Solid Films* **2002**, *411*, 147.

(41) Hiramatsu, H.; Ueda, K.; Ohta, H.; Orita, M.; Hirano, M.; Hosono, H. *Appl. Phys. Lett.* **2002**, *81*, 598.

(42) Hiramatsu, H.; Ohta, H.; Suzuki, T.; Honjo, C.; Ikuhara, Y.; Ueda, K.; Kamiya, T.; Hirano, M.; Hosono, H. *Cryst. Growth Des.* **2004**, *4*, 301.

(43) Hiramatsu, H.; Ueda, K.; Takafuji, K.; Ohta, H.; Hirano, M.; Kamiya, T.; Hosono, H. *J. Mater. Res.* **2004**, *19*, 2137.

(44) Hiramatsu, H.; Ohta, H.; Hirano, M.; Hosono, H. *Solid State Commun.* **2002**, *124*, 411.
(45) Blaha, P.; Schwarz, K.; Madsen, G.; Kvasnicka, D.; Luitz, J. WIEN2k, An Augmented Plane Wave + Local Orbitals Program for Calculating Crystal Properties. Karlheinz Schwartz, Techn. Universität Wien, Austria, 2001.
(46) Varshni, Y. P. *Physica* **1967**, *34*, 149. The model is described as follows; $E(T) = E(0) - \alpha T^2/(T + \beta)$, where $E(T)$ is the exciton energy at T (K), and $E(0)$, α, and β are the fitting parameters.
(47) Hess, S.; Taylor, R. A.; Ryan, J. F.; Beaumont, B.; Gibart, P. *Appl. Phys. Lett.* **1998**, *73*, 199.
(48) Watanabe, H.; Hayashi, K.; Takeuchi, D.; Yamanaka, S.; Okushi, H.; Kajimura, K.; Sekiguchi, T. *Appl. Phys. Lett.* **1998**, *73*, 981.
(49) Kokalj, A. *J. Mol. Graphics Model.* **1999**, *17*, 176.
(50) Kawazoe, H.; Ueda, K. *J. Am. Ceram. Soc.* **1999**, *82*, 3330.
(51) Dimmock, J. O.; Wheeler, R. G. *J. Appl. Phys.* **1961**, *32*, 2271.
(52) Wheeler, R. G.; Dimmock, J. O. *Phys. Lev.* **1962**, *125*, 1805.
(53) O′donnell, K. P.; Parbrook, P. J.; Henderson, B.; Trager-Cowan, C.; Chen, X.; Yang, F.; Halsall, M. P.; Wright, P. J.; Cockayne, B. *J. Cryst. Growth* **1990**, *101*, 554.
(54) Murray, C. B.; Norris, D. J.; Bawendi, M. G. *J. Am. Chem. Soc.* **1993**, *115*, 8706.